Research of photonic-assisted triangular-shaped pulses generation based on quadrupling RF modulation*

YUAN Jin (袁瑾), **NING Ti-gang** (宁提纲), **LI Jing** (李晶)**, **LI Yue-qin** (李月琴), **CHEN Hong-yao** (陈宏尧), **and ZHANG Chan** (张婵)

Institute of Lightwave Technology, Beijing Jiaotong University, Beijing 100044, China

(Received 29 September 2014; Revised 7 November 2014)

We propose an approach to generate optical triangular-shaped pulse train with tunable repetition rate using quadrupling radio frequency (RF) modulation and optical grating dispersion-induced power fading. In this work, a piece of chirped fiber Bragg grating (FBG) is employed as the dispersive media to remove the undesired 8th harmonic in optical intensity. Thus, the generated harmonics of optical intensity can be corresponding to the first two Fourier components of typical periodic triangular pulses. This work also analyzes the impacts of the extinction ratio and the bias voltage drift on the harmonic distortion suppression ratio. After that, the value of the extinction ratio and the range of the bias voltage drift can be obtained. The advantage of this proposal is that it can generate high order frequency-multiplexed optical pulses train which can be applied in all optical signal processing and other fields.

Document code: A **Article ID:** 1673-1905(2015)03-0207-6

DOI 10.1007/s11801-015-5018-x

Optical triangular-shaped pulse has many applications, such as all-optical data processing[1-4]. Therefore, the photonic triangular-shaped pulse generator is considered to be an imperative device for future all-optical network. In recent years, a series of research achievements about triangular-shaped optical pulses generator have been reported internationally[5-9]. All-optical pulse shaping using mode-locked lasers as the light source is currently the most common approach to obtain the symmetrical triangular-shaped optical pulses. For example, in Ref.[5], J. Ye et al mentioned a popular approach which is based on optical-spectrum-shaping method combined with frequency-to-time mapping. In 2013, A. Zhang et al[6] researched that arbitrary waveform, such as symmetrical triangular-shaped optical pulse, can be generated by using three grating arrays as spectrum shaping unit. B. Dai et al[7,8] carried out a versatile waveform generator based on frequency comb generation. In addition, J. Li et al[9] reported and analyzed a generator based on harmonic fitting.

This paper elaborates a method to generate periodic triangular pulse through theoretical analysis and simulation. A triangular pulse train with tunable repletion rate is generated. Since the quadrupling RF modulation technique is employed, repetition rate of the target pulse train is four times of the driving frequency.

Fig.1 shows the schematic setup of triangular-shaped pulses generation based on quadrupling RF modulation. A lightwave from a continuous-wave (CW) laser is transmitted to a dual-parallel Mach-Zehnder modulator (MZM). The RF signal generated by a vector signal generator is divided into two parts by a 90° hybrid coupler and then imported to two sub-MZMs (MZ-a and MZ-b, each has independent DC bias) of the DP-MZM. The modulator is operated at push-pull mode. Then, three bias voltages of DP-MZM should be carefully manipulated to make sure that the modulator is under quadrupling RF modulation. Simultaneously, MZ-a and MZ-b should be biased at maximum transmission point (MATP), and MZ-c should be biased at minimum transmission point (MITP). Finally, a chirped fiber Bragg grating (CFBG) is used to manipulate the achieved signal. By properly choosing the dispersion of the CFBG, the undesired harmonic can be suppressed.

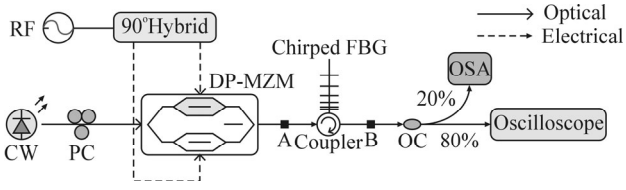

Fig.1 Schematic setup of the proposed generator

The mechanism of quadrupling RF modulation technology is expressed as below. The RF signal considered as $V_{RF}\cos(\omega_{RF}t)$ is operated at an amplitude of V_{RF} and a frequency of $\omega_{RF}/2\pi$ to drive the DP-MZM. When the extinction ratio of DP-MZM is assumed to be infinite

* This work has been supported by the Fundamental Research Funds of the Central Universities (No.2015YJS004).

** E-mail:lijing@bjut.edu.cn

($\varepsilon_r=\infty$), the optical field at the output of DP-MZM (point A in Fig.1) can be shown as

$$E_A(t)=\frac{E_{in}(t)}{2}\left\{\exp\left[\mathrm{j}\frac{V_{RF}}{2V_\pi}\cos(\omega_{RF}t)\right]+\exp\left[-\mathrm{j}\frac{V_{RF}}{2V_\pi}\cos(\omega_{RF}t)\right]-\exp\left[-\mathrm{j}\frac{V_{RF}}{2V_\pi}\sin(\omega_{RF}t)\right]-\exp\left[\mathrm{j}\frac{V_{RF}}{2V_\pi}\cos(\omega_{RF}t)\right]\right\}=\frac{E_{in}(t)}{2}\sum_{k=-\infty}^{\infty}a_{4k-2}\exp\left[\mathrm{j}(4k-2)\omega_{RF}t\right], \quad (1)$$

where $a_{4k-2}=[\mathrm{j}^{4k-2}+\mathrm{j}^{4k-2}(-1)^{4k-2}-(-1)^{4k-2}-1]J_{4k-2}(m)$, V_π represents the half-wave switching voltage and $E_{in}(t)=E_0\exp(\mathrm{j}\omega_0 t)$ denotes the optical field at the input of the DP-MZM. E_0 and ω_0 are the amplitude and angular frequency respectively. Fig.2 gives the relationship between the first kind of Bessel function and the corresponding modulation index, $m=\pi V_{RF}/2V_\pi$. By tuning m to 4.438, $J_2(m)\approx 3J_6(m)$ is satisfied. Moreover, the impact of the 10th order harmonic is negligibly small.

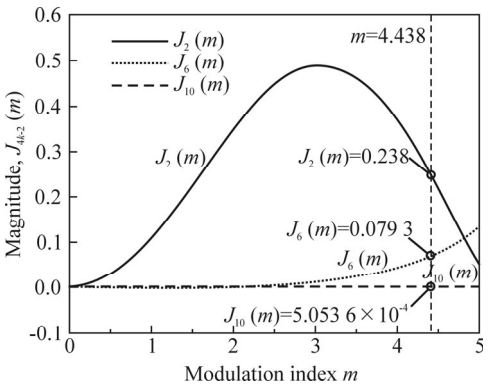

Fig.2 Bessel function of the first kind with order of $4k$-2, $J_{4k-2}(m)$ versus modulation index m[10]

Thus, the optical field of point A can be simplified as

$$E_A(t)\approx\frac{E_{in}(t)}{2}\left[a_{-6}\exp(-\mathrm{j}6\omega_{RF}t)+a_{-2}\exp(-\mathrm{j}2\omega_{RF}t+a_2\exp(\mathrm{j}2\omega_{RF}t)+a_6\exp(\mathrm{j}6\omega_{RF}t)\right]. \quad (2)$$

The corresponding optical field intensity can be written as

$$I_A(t)\propto\left[\left(a_{-6}^2+a_{-2}^2+a_2^2+a_6^2\right)+2\left(a_{-2}a_2+a_{-6}a_{-2}+a_{-2}a_{-6}\right)\cos\left(4\omega_{RF}t\right)+2\left(a_{-6}a_2+a_{-2}a_6\right)\cos\left(8\omega_{RF}t\right)+2a_{-6}a_6\cos\left(12\omega_{RF}t\right)\right]. \quad (3)$$

It is found that there exist only three RF components (4th, 8th and 12th order harmonics) in the optical intensity. This scheme substitutes the single-mode fiber for a CFBG to import the dispersion D_gL_g. Afterwards, the optical field at the output of the grating (point B) can be expressed as

$$E_B(t)\propto\left[a_{-6}\exp\left(-\mathrm{j}6\omega_{RF}t+\mathrm{j}18\xi\omega_{RF}^2\right)+a_{-2}\exp\left(-\mathrm{j}2\omega_{RF}t+\mathrm{j}2\xi\omega_{RF}^2\right)+a_2\exp\left(\mathrm{j}2\omega_{RF}t+\mathrm{j}2\xi\omega_{RF}^2\right)+a_6\exp\left(\mathrm{j}6\omega_{RF}t+\mathrm{j}18\xi\omega_{RF}^2\right)\right], \quad (4)$$

where $\xi=(-\lambda_0^2/2\pi c)D_gL_g$. Its corresponding optical field intensity becomes

$$I_B(t)\propto\left[\left(a_{-6}^2+a_{-2}^2+a_2^2+a_6^2\right)+2a_{-2}a_2\cos\left(4\omega_{RF}t\right)+2a_{-6}a_6\cos\left(12\omega_{RF}t\right)+4a_2a_6\cos\left(16\xi\omega_{RF}^2\right)\cos\left(8\omega_{RF}t\right)\right]. \quad (5)$$

In order to remove the undesired 8th harmonic, the dispersion of the CFBG must meet the following requirement:

$$D_gL_g=\left(\frac{2n+1}{2}\right)\frac{c\pi^2}{8\omega_{RF}^2\lambda_0^2},\ n=0,\ 1,\ 2\cdots, \quad (6)$$

where λ_0, c, L_g, D_g represent central wavelength, speed of light in vacuum, fiber length and dispersion parameter, respectively. Then substituting Eq.(5) into Eq.(1), the output optical intensity can be calculated as

$$I_{out}(t)\propto\cos(4\omega_{RF})+\frac{J_6^2(m)}{J_2^2(m)}\cos(12\omega_{RF}t)\quad . \quad (7)$$

The Fourier expansion of ideal triangular-shaped waveform can be expressed as

$$T(t)\propto\sum_{i=1}^{\infty}\frac{1}{(2i-1)^2}\cos\left[(2i-1)\Omega t\right]=\cos(\Omega t)+\frac{1}{9}\cos(3\Omega t)+\frac{1}{25}\cos(5\Omega t)+\cdots. \quad (8)$$

Fig.3 illustrates the calculated gradient of $T(t)$ when i is tuned to 2, 4, 8 respectively. It is shown that the gradients are approximately constant across the up-and-f alling edge of the pulse train once the coefficient i is equal to 8. Considering the energy of triangle-shaped pulse is concentrated on low frequencies and the attenuation of higher order components is fast, we can regard the impact of high order harmonic on the generated triangular pulse is negligible small. Thus, we can enable i=2 in Eq.(8). Assuming $\Omega=4\omega_{RF}$, for a given modulation index m=4.438, $J_6^2(m)/J_2^2(m)$=1/9 can be obtained. Comparing Eq.(7) with Eq.(8) again, we can conclude that the weight of every order harmonic of optical field intensity is identical to the Fourier expansion of ideal

triangular-shaped waveform.

Fig.4 presents temporal waveform calculated from $T(t)$ and $I_{out}(t)$. It is found that the triangular waveform is pretty close to ideal triangular waveform, which illustrates that using the first two order harmonic fitting can approximately express the temporal characteristics of triangular-shaped pulses.

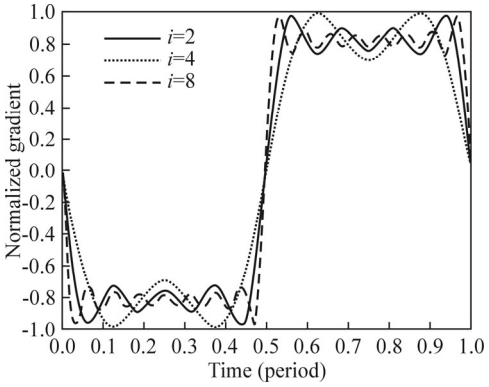

Fig.3 Calculated normalized gradient of $T(t)$ at i=2, 4, 8

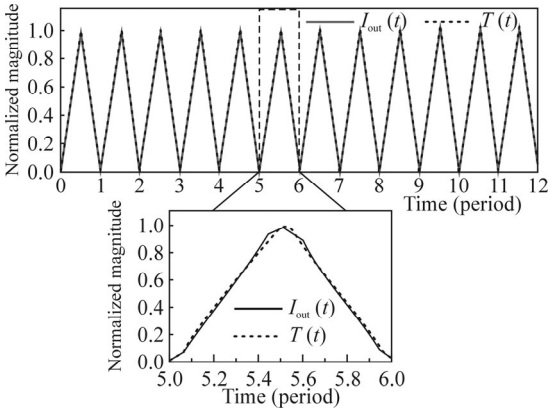

Fig.4 Calculated temporal waveforms of $T(t)$ and $I_{out}(t)$

To investigate the mechanism, simulations are carried out via Optisystem software package. The simulations are conducted according to the schematic setup as shown in Fig.1. An optical signal from a CW laser at central wavelength of 1 550 nm and linewidth of 0.8 MHz is sent to a DP-MZM. The DP-MZM has insertion loss of 5.5 dB, half-wave switching voltage of 4 V and extinction ratio of 25 dB. The DC biases of two sub-MZMs of the DP-MZM are set to MATP, MATP and that of the parent MZM is set to MITP. By changing the magnitude of the electrical signal, modulation index m can be tuned to 4.438. Subsequently, the achieved signal is transmitted by a CFBG. Owing to the finite extinction ratio, the odd order sidebands such as ±1st, ±3rd, ±5th and ±7th will affect the temporal waveform. This impact can be minimized via appropriately adjusting the dispersion coefficient of the CFBG. In Ref.[10], the minimum disturbance can be obtained when n=5. Thus, Eq.(5) can be simplified as $D_gL_g=11\pi^2c/16\omega_{RF}^2\lambda_2$. Taking f_{RF}=10 GHz for example, the required grating dispersion is D_gL_g=214.47 ps/nm.

Fig.5 shows the temporal simulation waveform of optical intensity $I_{out}(t)$ before and after inserting the CFBG. Fig.5(a) shows that before the CFBG is inserted, the up-and-falling edge of triangular pulse is increasing slowly and it has no linear variation. The reason is that before the CFBG is imported, the 8th harmonic components of the optical intensity may destroy the entire temporal characteristics. After inserting the CFBG, dispersion-induced power fading can eliminate the effect caused by the 8th harmonic, and the high-quality periodic triangular pulse will be generated as shown in Fig.5(b).

The optical spectrum and electrical spectrum of output optical field intensity $I_{out}(t)$ are presented in Fig.6. As shown in Fig.6(a), the sideband power difference between the ±2nd and the ±6th is approximately 9.5 dB, which satisfies $J_6^2(m)/J_2^2(m)$=1/9. In Fig.6(b), the power difference between the 4th and the 6th harmonics turns out to be 19.08 dB, which also agrees well with the previous discussion. To evaluate the impact of the undesired harmonics, a harmonic distortion suppression ratio (HDSR) is defined as the power ratio of 4th order harmonic and the harmonics with maximum interference. Absolutely, a larger HDSR means less interference. Due to the application of quadrupling RF modulation technology, when the driving frequency is chosen as f_{RF}=10 GHz, a triangular pulse with frequency of 40 GHz and period of 25 ps can be generated. In addition, the parameters of the CFBG and DP-MZM may affect the performance of the scheme as the following discussions.

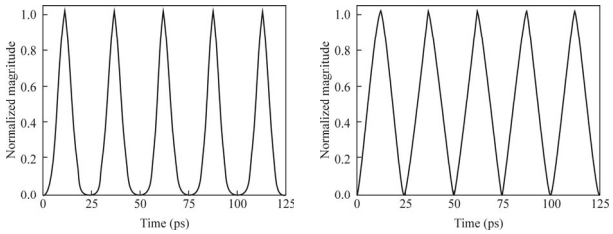

Fig.5 Shape evolutions of optical intensity $I_{out}(t)$ (a) before and (b) after CFBG transmission

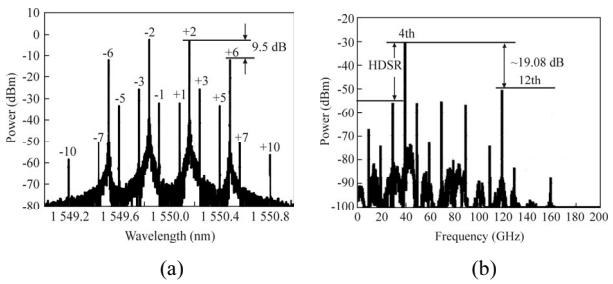

Fig.6 Simulated results of optical intensity at f_{RF}=10 GHz, D_gL_g=214.47 ps/nm: (a) Optical spectrum; (b) Electrical spectrum

The dispersion of pulses transmitted in a fiber can be compensated by a CFBG, enabling the pulses to restore the original condition. Hence, it is feasible to substitute a CFBG for the single-mode fiber. Thus, it is essential to discuss the chirp coefficient C, the length L_g and the modulation depth δn of the CFBG to select the available grating. According to the fiber grating dispersion coefficient definition $D=\Delta T/(L_g\Delta\lambda)$ and the time a light transmits a round trip in a grating is $\Delta T=2L_g n_{eff}/c$, the dispersion coefficient proves to be $D_g=2n_{eff}/\Delta\lambda c$, where $\Delta\lambda$ denotes the wavelength bandwidth of the CFBG and $n_{eff}\approx1.46$ represents the effective refractive index. When D_gL_g=214.47 ps/nm, the desired chirp coefficient of the CFBG is $C=\Delta\lambda/L_g$=0.457 nm/cm.

Fig.7 presents the reflectivity spectrum and time-delay curve of the CFBG at different lengths when the modulation depth is chosen as δ_n=0.000 5. As shown in the figure, for a given modulation depth δ_n, the bandwidth of the reflectivity spectrum gets larger along with the increase of the grating length. And within reflection bandwidth, the slope of the time-delay curve stays invariant and the time-delay jitter is also basically constant. However, as the length increases, the jitter at the top of the reflection spectrum becomes weakened. As a result, a CFBG with larger length is more preferred. Similarly, Fig.8 shows the reflection spectrum and time-delay curve of the CFBG at a length of 8 cm with variable modulation depth δ_n. Note that the modulation depth has a marked impact on the spectral distribution. When δ_n becomes lager, the reflectivity slightly increases and the reflectivity spectrum of the CFBG becomes wider. Meanwhile, the overall slope of the grating time-delay curve has little change, while the grating delay jitter within reflection bandwidth gets stronger which will result in the larger distortion of the generated triangular wave finally. Therefore, CFBG with less modulation depth is much preferred. In summary, the CFBG which is characterized by C=0.457 nm/cm, L_g=8 cm, δ_n=0.000 5 is used to generate the triangular-shaped optical pulses with better performance in this scheme.

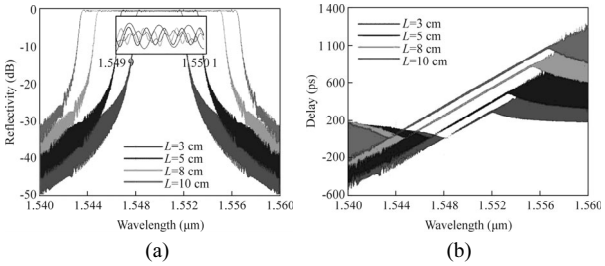

Fig.7 Simulated (a) reflectivity spectra and (b) time-delay curves at different CFBG lengths

Besides, the finite extinction ratio will affect the temporal characteristics of the optical pulse, which makes an effect on the performance of the triangular-shaped optical pulse generator. Here, HDSR will be discussed to verify the impact of the finite extinction ratio on this scheme. According to the previous analysis, temporal waveform of $I_{out}(t)$ relies on the relationship between the 4th and the 12th harmonics. Only when $P_{4\Omega}/P_{12\Omega}$ is approximately equal to 19.08 dB, can stable triangular pulse train be obtained. Fig.9 displays the simulated $P_{4\Omega}/P_{12\Omega}$ and HDSR versus different extinction ratios. When ε_r is varied from 10 dB to 35 dB, $P_{4\Omega}/P_{12\Omega}$ is varied within the range of 5% from 19.08 dB. But when ε_r is lower than 20 dB, the HDSR is lower than 19.08 dB, which means the power of the interference harmonic is higher than that of the 12th harmonic. With the increasing of ε_r, the value of HDSR becomes larger and the distortion decreases. It meets the scheme requirements when ε_r is higher than 25 dB. Consequently, we use electro-optic modulator with larger extinction ratio which can reduce the impact of finite extinction ratio on scheme performance to obtain stable triangular pulse.

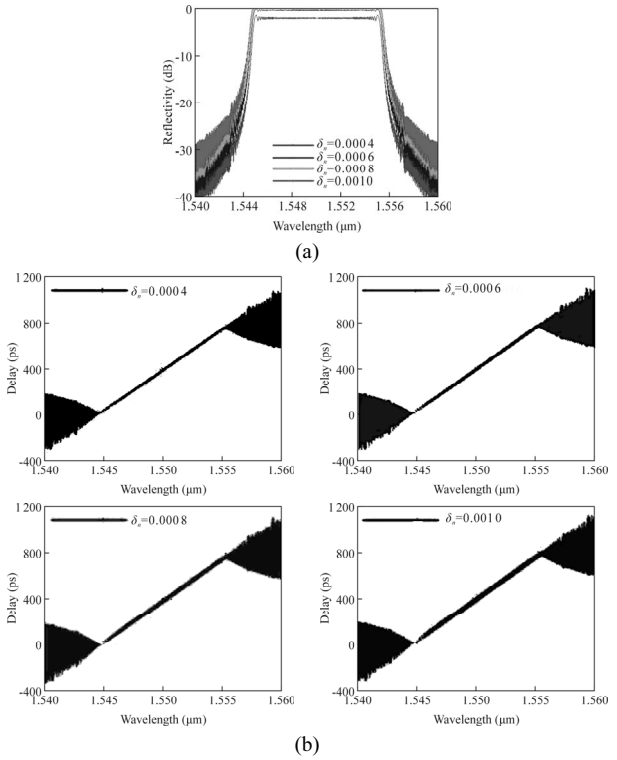

Fig.8 Simulated (a) reflectivity spectra and (b) delay curves at different modulation depths

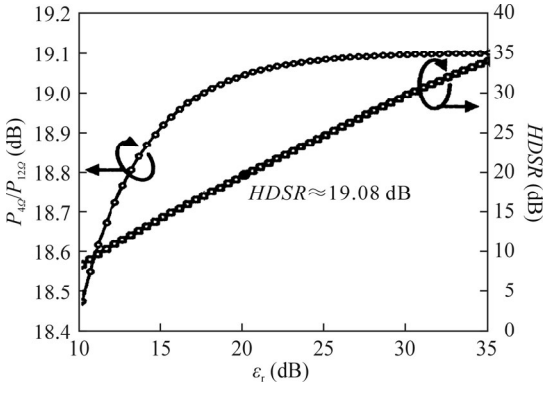

Fig.9 Simulated $P_{4\Omega}/P_{12\Omega}$ and *HDSR* versus extinction ratio

In addition, the scheme has imported a DP-MZM of which the bias drift can influence $P_{4\Omega}/P_{12\Omega}$ and HDSR. The DP-MZM in this scheme possesses three independent bias voltages and they are stabilized at MATP, MATP and MITP respectively. In order to verify the impact caused by the bias drift, this paper discussed the three bias voltage drifts respectively. The parameter $\Delta V_{\text{bias}}=(\Delta V/V_{\pi})\times 100\%$ is defined as the bias drift. Taking ε_r=25 dB for example, Fig.10 shows $P_{4\Omega}/P_{12\Omega}$ and HDSR versus MZM-a bias drift and MZM-b bias drift. As analyzed from the figure, when ΔV_{bias} varies from −10% to +10%, $P_{4\Omega}/P_{12\Omega}$ almost remains constant while HDSR decreases from 25 dB to 10 dB. Assuming when the variation of HDSR is within the range of 5% from 25 dB, the caused distortion is acceptable. In this case, the bias drifts of MZM-a and MZM-b prove to be $-1\%\le\Delta V_{\text{bias}}\le 0.5\%$. Fig.10(c) shows $P_{4\Omega}/P_{12\Omega}$ and HDSR versus the MZM-c bias drift. The tolerable range of the bias drift is $-1\%\le\Delta V_{\text{bias}}\le 1\%$. In practical applications, combining modulator with larger half-wave voltage with bias voltage circuit can stabilize the mentioned three bias voltages within an acceptable range.

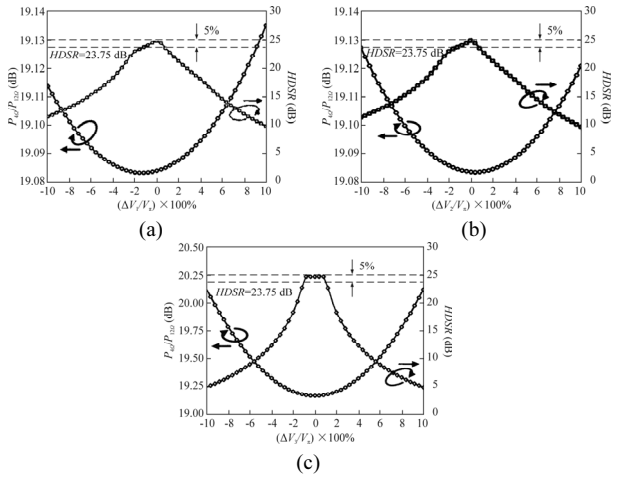

Fig.10 Simulated $P_{4\Omega}/P_{12\Omega}$ and *HDSR* versus MZM bias voltage: (a) MZM-a bias drift; (b) MZM-b bias drift; (c) MZM-c bias drift

To investigate the repetition rate's tunability, we simulate the temporal waveform of $I_{\text{out}}(t)$ with various driving frequencies. According to the expression of Eq.(5), repetition rate's tunability can be realized by tuning driving frequency f_{RF} and grating dispersion D_gL_g. When f_{RF} is tuned to 7.5 GHz, 10 GHz, 12.5 GHz and 15 GHz, the corresponding dispersion D_gL_g is supposed to be adjusted to 381.28 ps/nm, 214.47 ps/nm, 137.26 ps/nm and 95.32 ps/nm, respectively. As shown in Fig.11, the generated triangular-shaped optical pulse train has tunable repetition rate which is four times of the driving frequency because of the quadrupling RF modulation applied in the proposal. Ultimately, even if the driving frequency gets small, pulse train with high repetition rate could still be generated, which expands the tuning range of the triangular-shaped optical pulse train.

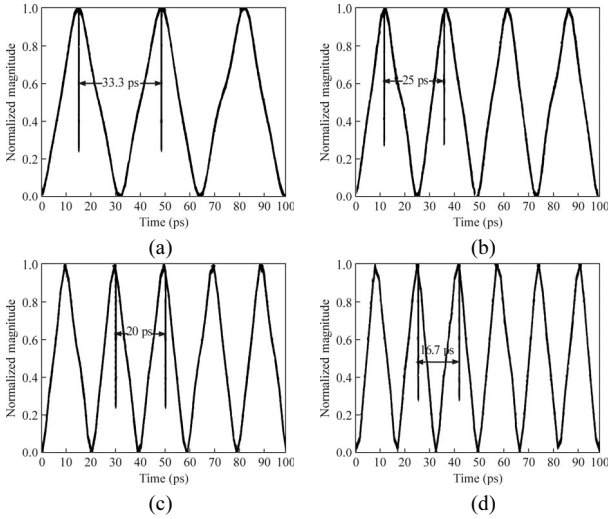

Fig.11 Simulated temporal waveforms of optical intensity with repetition rates of: (a) 30 Gbit/s, (b) 40 Gbit/s, (c) 50 Gbit/s and (d) 60 Gbit/s

In this paper, an optical triangular-shaped pulse train generation approach using quadrupling RF modulation incorporating optical grating dispersion-induced power fading has been proposed. The generated triangular-shaped optical pulse train has tunable repetition rate which is four times of the driving frequency. Firstly, we through calculating the chirp coefficient C and discussing the impacts of the optical grating length L_g and its modulation depth δ_n on the grating reflectivity spectrum and the time-delay curve to select the required grating. Further, simulations have been taken to evaluate the impact of finite ε_r and bias drift ΔV_{bias}. It is found that when ε_r within the range from 20 dB to 35 dB, $P_{4\Omega}/P_{12\Omega}$ basically remains at 19.08 dB and HDSR is higher than 19.08 dB, which can be considered as the characteristics of triangle pulse. With the increase of ε_r, the temporal waveform is more close to the ideal triangular pulse. In addition, the impact of the bias drift of the DP-MZM on $P_{4\Omega}/P_{12\Omega}$ and HDSR has been researched. The bias voltage drifts of two sub-MZMs of the DP-MZM must be within a range from −1% to 0.5% while the bias voltage drift of the parent MZM must be from −1% to 1%. These discussions make the scheme more practical. Finally, a triangular pulse train with tunable repletion rate can be achieved by tuning the driving frequency and the grating dispersion.

References

[1] F. Parmigiani, M. Ibsen and T. T. Ng, Efficient Optical Wavelength Conversion Using Triangular Pulses Generated Using a Superstructured Fiber Bragg Grating, 2008 Optical Fiber Communication Conference, San Diego, CA, USA, 2008.

[2] R. S. Bhamber, A. I. Latkin and S. Boscolo, All-optical TDM to WDM Signal Conversion and Partial Regeneration Using XPM with Triangular Pulses, the

34th European Conference on Optical Communication, Brussels, Belgium, 2008.

[3] A. I. Latkin, S. Boscolo and R. S. Bhamber, Optical Frequency Conversion, Pulse Compression and Signal Copying Using Triangular Pulses, the 34th European Conference on Optical Communication, Brussels, Belgium, 2008.

[4] A. I. Latkin, S. Boscolo and R. S. Bhamber, Opt. Soc. Am. B **26**, 1492 (2009).

[5] Ye J, Yan L and Pan W, Optics Letters **36**, 1458 (2011).

[6] A. Zhang and C. Li, Optics & Laser Technology **52**, 81 (2013).

[7] B. Dai, Z. Gao and X. Wang, Electronics Letters **47**, 336 (2011).

[8] B. Dai, Z. Gao and X. Wang, IEEE/OSA Journal of Lightwave Technology **31**, 145 (2013).

[9] J. Li, X. Zhang and B. Hraimel, IEEE/ OSA Journal of Lightwave Technology **30**, 1617 (2012).

[10] J. Li, T. Ning and L. Pei, Optical Fiber Technology **19**, 574 (2013).

[11] Erdogan T., Journal of Lightwave Technology **15**, 1277 (1997).

[12] ZHANG Zi-jia, Fiber Grating Theoretical Basis, Science Press, Beijing, 2009. (in Chinese)